To appear in: **Majlesi Journal of Electrical Engineering (MJEE)**

Online ISSN: 2345-377X **Print ISSN:** 2345-3796

Received: 16-Jan-2025 Revised: 20-Feb-2025

Accepted: 27-Apr-2025

DOI: 10.57647/j.mjee.2025.16846

Original Research

Title: Enhanced Navigation Accuracy Using Nonlinear Kalman Filters in INS/GPS Integration

Mohammadreza Mollaei[1], Mohsen Shafieirad[2], Elahe Moradi[3]

1- Department of Electrical and Computer Engineering, University of Kashan, Kashan, Iran.

Email: mohammadreza_mollaei1@yahoo.com

2- Department of Electrical and Computer Engineering, University of Kashan, Kashan, Iran.

Email: m.shafieirad@kashanu.ac.ir (**Corresponding author**)

https://orcid.org/0000-0002-3239-8987

3- Department of Electrical Engineering, YI.C., Islamic Azad University, Tehran, Iran.

Email: elahemoradi@iau.ac.ir

Abstract

This study explores the challenges of error accumulation in inertial navigation systems (INS) and presents a solution to enhance navigation accuracy. To address these errors, INS data is integrated with GPS using advanced nonlinear Kalman filters, specifically the Unscented

Kalman Filter (UKF) and the Particle Kalman Filter (PKF). These methods are applied to a six-degree-of-freedom fixed-wing aircraft model, and their performance is evaluated under both GPS-enabled and GPS-denied conditions. The results show that nonlinear filters, particularly the PKF, outperform the Extended Kalman Filter (EKF) in providing accurate position and velocity estimates, while also preventing system divergence during GPS outages. This study confirms that integrating INS and GPS with advanced nonlinear filters can significantly enhance navigation accuracy and reliability.

KEYWORDS: Nonlinear Kalman filter, Particle Kalman Filter, Inertial Navigation, GPS Outage

INTRODUCTION

The navigation system is one of the main and most important parts of the positioning system in controlling guidance systems. The main purpose of navigation is to determine the geographical position (longitude, latitude, and altitude), speed (speed components in the navigation device), and position (elevation and direction angles) of a vehicle. In [1], the authors examine the navigation of an air autopilot in areas without GPS. This method an error state extended Kalman filter (ES -EKF) is used in this paper. In [2], deal with the navigation of micro-aerial vehicles when GPS is down. This paper is devoted to software redesign and software architecture for a better understanding of the autopilot environment. In [3], the authors discussed the danger of GPS disconnection for drones. It uses the UKF filter to provide support for GPS-deprived areas by reprogramming. In [4], the authors design a navigation system for a ground vehicle. This system combines omnidirectional vision sensors with INS and GPS systems. In [5], to be more confident in the integrated navigation capability even when the GPS is disconnected, it uses the dual navigation model based on square root and random forest regression. In [6], it deals with improving the gyroscope and MEMS sensors to solve the navigation problem. It provides a bandwidth expansion method with an extended temperature range for the gyroscope and MEMS sensor. In another [7], to improve the detection of apparent motion from the accelerometer, a parameter identification and reconstruction algorithm is presented.

In [8], an auxiliary gyroscope is used to determine the relative attitude between the objects on the moving base and the reference system. The main gyroscope is for sensing the entire movement and the auxiliary gyroscope is for the movement of the moving base. This paper deals with the navigation of a land vehicle. To improve the performance, the authors used the PKF along with the neural network-based method to improve the INS error at the time of disconnection and connection of GPS [9]. In [10], to improve the performance of the integrated INS and GPS, a modified Kalman filter is presented to reduce the computations. In [11], a localization solution (IMM-UKF) is proposed for ground vehicles that can simultaneously adapt to unknown noise with INS sensors and communicate with the GPS. The authors of [12] used the cubic Kalman (CKF) filter for optimal

sensitivity to the information obtained from the observations. In [13] on autonomous driving systems, a hybrid approach is proposed to solve the problem of vehicle position prediction in partial and complete GPS outages. The proposed method collects the advantages of the fuzzy inference system (FIS) and the random Gaussian model (SRG) and is called FIS-SRG as a result. In [14], because the performance of the navigation system may decrease in the presence of model errors, the H-infinity filter is used to remove the effects of model errors to check uncertainties or minimize the estimation error. [15] is presented for the integration of a global positioning system (GPS) and inertial navigation system (INS) during GPS disconnection, in this method Kalman filter with multiple reduction factor (MDF-CKF) and random forest (RF) is presented.

In [16], to increase the performance of the navigation system (INS/GPS) when the GPS is disconnected, a new model is presented that directly relates the speed and angular rate of the INS to the increase of the GPS position. In this paper, the Kalman filter and multilayer perceptron (MLP) network are used in combination. In [17], a learning algorithm based on the neural network method is proposed for complex data caused by irregular vehicle movements. In [18], the method of unbiased finite impulse response (UFIR) and Kalman filter based on an adaptive interactive multiple model (IMM) is proposed to provide accurate position information of a mini quadrotor. In [19], the authors discussed the autonomous navigation of micro aerial vehicles in environments without GPS. A perception system is proposed to localize and understand the environment and a motion planning and control system to avoid collision is also presented.

[20] is presented to improve positioning performance by suppressing effective random noise in gyroscopes using a nonlinear suppression method based on the Cubature Kalman Filter-Phase Space Reconstruction method (CKF-PSR). In [21], the use of sigma-point-based Kalman filters is proposed for nonlinear filter problems, and this method is also proposed for the cubic Kalman filter (CKF) as an ideal solution for the system GNSS/INS. Navigation systems play a pivotal role in determining the position, velocity, and orientation of vehicles across a variety of platforms, from autonomous drones to underwater vehicles. While GPS provides highly accurate global positioning, its performance can degrade significantly in environments with signal interruptions, such as urban canyons, forests, or underwater operations. Inertial Navigation Systems (INS), with their self-contained nature, offer a complementary solution to GPS, providing continuous navigation without reliance on external signals. However, standalone INS suffers from error accumulation over time, necessitating integration with GPS for reliable performance. Recent advancements have enhanced the synergy between INS and GPS. For instance, robust integration methods using Low Earth Orbit (LEO) satellites have demonstrated improved geometric configurations and positioning accuracy in GPS-degraded environments. These approaches, combined with robust Kalman filtering techniques, have significantly reduced errors, offering better continuity in navigation [22].

Additionally, innovations in strap down INS technology have minimized size, cost, and mechanical complexity, making it suitable for a broader range of applications [23]. Emerging technologies like deep learning are also reshaping navigation. Machine learning techniques are now being applied

to enhance sensor fusion, improve noise compensation, and optimize filter parameters in real-time, pushing the boundaries of accuracy and computational efficiency in INS/GPS systems . In a paper explores the integration of INS and GPS using advanced nonlinear filters, with a focus on their application in complex navigation scenarios. Inertial navigation systems (INS) have gained significant importance in autonomous navigation, providing reliable position and velocity information. However, their accuracy can degrade over time due to cumulative errors, especially in GPS-deprived environments. To mitigate this, advanced nonlinear filters such as the Unscented Kalman Filter (UKF) and Particle Kalman Filter (PKF) have been developed to enhance state estimation in complex navigation scenarios [24]. Recent studies have explored robust Kalman filtering techniques tailored to manage model uncertainties and measurement outliers. For instance and introduced a distributional robust Kalman filter that improves tightly coupled INS/GPS integration under high uncertainty. Similarly, augmented quaternion-based UKF models have been proposed to increase the accuracy of loosely coupled INS/GPS systems by incorporating quaternion representations, which are particularly beneficial for dynamic systems [25].

Many studies have been conducted on adaptive Kalman filters in the past decades. However, it is always challenging to achieve online estimation with high estimation accuracy and fast convergence speed. In order to design online MLE-based AKFs with high estimation accuracy and fast convergence speed, an online heuristic MLE approach is proposed in a paper, based on which a small-coordinate descending noise covariance estimation framework is developed[26]. Adaptive Kalman filters have many applications and solve many challenges, including online estimation of the process noise covariance matrix [27]. In many cases, estimation methods are not able to detect outliers and are only able to measure the current points. In a paper to solve this problem, a measurement interval is used for better detection. Also, with the help of an adaptive method, it leads to an accurate Kalman filter [28]. Global Navigation Satellite Systems (GNSS) are prone to intermittent outages. In this paper, we use non-holonomic constraints (NHC) to improve navigation accuracy [29]. In autonomous systems, microelectromechanical systems (MEMS) and multiple sensors are usually used to achieve high-precision positioning. However, for many reasons, navigation sensors may not be accurate enough. In one paper, a multi-model (IMM) inertial navigation system approach is used to solve this problem [30].

PKF excels in environments with high uncertainty or non-Gaussian noise, such as extended GPS outages or when sensor measurements are highly corrupted. By employing particle filtering, PKF can model non-Gaussian distributions and adapt more effectively to abrupt changes or anomalies in the system dynamics, providing a more reliable estimate than CKF. The PKF leverages the strengths of both Kalman filtering and particle filtering, making it highly effective for complex nonlinear systems. Unlike CKF, which assumes Gaussian distributions and uses fixed sigma-point sampling, PKF dynamically samples the state space, enabling it to better approximate distributions in nonlinear scenarios. This capability is essential for scenarios involving rapid dynamics or irregular motion, where CKF's performance might degrade due to linearization limitations

In section 2, we determine the dynamic equations of the flying body. In section 3 nonlinear filter algorithms such as the UKF and the Particle Kalman filter (PKF) filter were used to integrate the data of the inertial navigation system with a navigation assistance system. In section 4, the results of simulations have been presented. The results indicate better performance of nonlinear filters to estimate and remove the inertial system error. Simulation is done in two modes of GPS and the results are compared. The combination of navigation systems is made to exploit their benefits and eliminate their disadvantages. Finally, the conclusion of this paper is presented in section 5.

In this article, we designed a real model based on real parameters and tested it in a scientific center and on a laboratory plant. The error was greatly reduced compared to the linear Kalman filter and we almost reached the boundary error. However, when using the linear Kalman filter, we observed complete divergence from the path when the GPS was disconnected in the laboratory plant.

In this paper, first, the dynamic structure is introduced, then the Kalman filter algorithm is presented, and after that, we will simulate different methods and compare them.

2. Dynamic equations of the flying body

To design a bird's flight control system, a mathematical model of the dynamic behavior of the bird's body is needed. In this section, the equations of motion and the force model are examined. As an example, and only as a visual representation, Figure 1 is considered to introduce the angles and coordinate axes of the flying object. The different parameters of the model are shown in this figure.

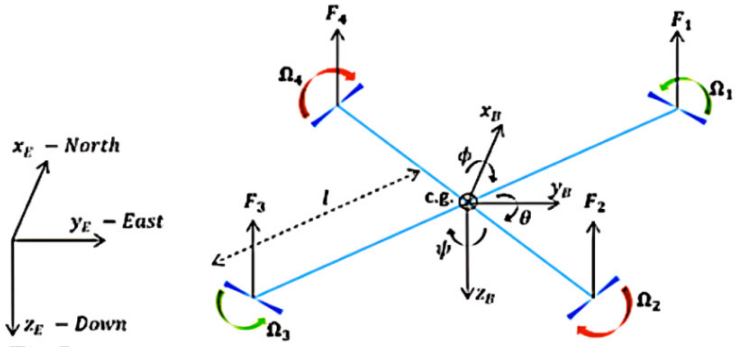

Fig1. Rotary wing air vehicle scheme [31]

Based on Figure 1, the dynamics of the bird can be written as first-order nonlinear differential equations as follows. Equation (1) represents the force equations:

$$\dot{v} = wp - ur + g \cdot sin\varphi cos\theta + \frac{F_y}{m} \tag{1}$$

$$\dot{u} = vr - wq - g \cdot sin\theta + \frac{F_x + T}{m} \tag{2}$$

$$\dot{w} = uq - vp + g \cdot cos\varphi cos\theta + \frac{F_z}{m} \tag{3}$$

Equation (2) shows the torque equations (angular velocities):

$$\dot{p} = \frac{I_z L + I_{xz} N}{I_x I_z - I_{xz}^2} + \frac{I_{xz}(I_x - I_y + I_z) + [I_z(I_y - I_z) - I_{xz}^2]qr}{I_x I_z - I_{xz}^2} \tag{4}$$

$$\dot{q} = \frac{1}{I_y}[M + pr(I_z - I_x) + I_{xz}(r^2 - p^2)] \quad (5)$$

$$\dot{r} = \frac{I_{xz}L + I_xN}{I_xI_z - I_{xz}^2} + \frac{[I_x(I_x - I_y) + I_{xz}^2]pq - [I_{xz}(I_x - I_y + I_z)]qr}{I_xI_z - I_{xz}^2} \quad (6)$$

Equation (3) expresses torque and aerodynamic forces.

$$L = \frac{1}{2}\rho V^2 sb[C_{l_\beta}\beta + C_{l_p}\frac{pb}{2V} + C_{l_{\delta_a}}\delta_a + C_{l_{\delta_r}}\delta_r] \quad (7)$$

$$M = \frac{1}{2}\rho V^2 s\bar{c}[C_{m_0} + C_{m_\alpha}\alpha + C_{m_q}\frac{\bar{c}q}{2V} + C_{l_{\delta_e}}\delta_e] \quad (8)$$

$$N = \frac{1}{2}\rho V^2 sb[C_{n_\beta}\beta + C_{n_p}\frac{pb}{2V} + C_{n_r}\frac{rb}{2V} + C_{n_{\delta_a}}\delta_a + C_{n_{\delta_r}}\delta_r] \quad (9)$$

In the above relationships, Fx, Fy and Fz are aerodynamic forces, T is propulsive force, Ix, Iy and Iz and Ixz are moments of inertial, φ, θ and ψ are attitude angles, α is the angle of attack, β is the angle of the lateral head, δa is the control surface of aileron, δe is the control surface of elevator, δr Rudder control surface, ρ air density, CL lift coefficient, CD drag coefficient, S wing reference surface, Q dynamic pressure, Cx, Cy and Cz, aerodynamic force coefficients, c¯average chord, b length Wing span and Cl, Cm and Cn are coefficients of aerodynamic moment. The following relations are obtained to calculate the linear velocity vector and angles of attack and lateral head.

$$\dot{\alpha} = q - (pcos\alpha + rsin\alpha)tan\beta - \frac{L}{mVcos\beta} + \frac{g}{Vcos\beta}(cos\varphi \cdot cos\theta \cdot cos\alpha + sin\theta \cdot sin\alpha) - \frac{Tsin\alpha}{mVcos\beta} \quad (10)$$

$$\dot{\beta} = psin\alpha - rcos\alpha + \frac{F_y cos\beta}{mV} + \frac{g}{V} \cdot cos\beta \cdot sin\varphi \cdot cos\theta + \frac{sin\beta}{V}(gcos\alpha \cdot sin\theta - gsin\alpha \cdot cos\varphi \cdot cos\theta - \frac{Tcos\alpha}{m} \quad (11)$$

$$\dot{V} = \frac{1}{m}[-Dc + mg(cos\varphi \cdot cos\theta \cdot sin\alpha.cos\beta + sin\varphi \cdot cos\theta \cdot sin\beta - sin\theta \cdot cos\alpha \cdot cos\beta) + Tcos\beta \cdot cos\alpha] \quad (12)$$

In the above formulas, L is the push force and D is the pull force. The obtained equations of motion are fixed for the coordinate system and it is not possible to describe the position and direction of the flying object relative to the fixed coordinate axes. The rotation around the z-axis of the body is the side angle ψ, the rotation around the y-axis of the body is the twist angle θ and the rotation around the x-axis of the body is the roll angle φ, the rate of change of the Euler angles can be obtained in terms of components of the angular velocity.

$$\dot{\varphi} = p + q \cdot sin\varphi \cdot tan\theta + r \cdot cos\varphi \cdot \tan\theta \quad (13)$$

$$\dot{\theta} = qcos\varphi - rsin\varphi \quad (14)$$

$$\dot{\psi} = qsin\varphi \cdot sec\theta - rcos\varphi \cdot sec\theta \quad (15)$$

In this case, absolute speed is expressed in terms of Euler angles and speed components in the body device.

$$\dot{x}_l = u\cos\theta \cdot \cos\psi + v(\sin\varphi \cdot \sin\theta \cdot \cos\psi - \cos\varphi \cdot \sin\psi) + w(\cos\varphi \cdot \sin\theta \cdot \cos\psi + \sin\varphi \cdot \sin\psi) \quad (16)$$

$$\dot{y}_l = u\cos\theta \cdot \sin\psi + v(\sin\varphi \cdot \sin\theta \cdot \sin\psi - \cos\varphi \cdot \cos\psi) + w(\cos\varphi \cdot \sin\theta \cdot \sin\psi + \sin\varphi \cdot \cos\psi) \quad (17)$$

$$\dot{z}_l = -u\sin\theta + v\sin\varphi \cdot \cos\theta + w\cos\varphi \cdot \cos\theta \quad (18)$$

3. DESIGNING OF EKF, UKF AND PKF

In this section, we intend to design the Kalman filter on the planet using the methods mentioned above, and simulate GPS in disconnected and connected states, and present the results.

In the INS/GPS integrated navigation system, the state variables of the Kalman filter include all the dynamic variables of the system that can be measured by sensors. For example, the state variables of the Kalman filter for the INS system, which consists of accelerometers and rate gyroscopes, include acceleration and rotation rate, which are determined by the relevant sensors. . Also, Kalman filter status variables for GPS navigation system include pseudo-distances, which are the distance between satellites and the receiving antenna, which determines the position coordinates of the GPS receiving antenna. This position can be in the form of longitude, latitude and geographic height relative to the elliptical earth or relative to the spherical earth or in the form of Cartesian coordinates in the ECEF or ECI device, etc. The Kalman filter consists of two stages: variable prediction update and variable correction. The correction stage causes the expression of the estimated state vector and the estimation error (covariance) and the Kalman gain, which is determined based on the new information obtained from the sensors and the estimated values for that time. Of course, it is also known as observation-based updating or measured updating. The prediction stage causes the expression of the guess state vector and the estimation error (covariance) using the system dynamics for the next time. Of course, it is also called as a temporary update.

In the complete integration method, the inertial navigation system is used as a reference path. For this purpose, when the GPS system has an output, the distance between the satellite and the receiver is calculated based on the output of the inertial navigation system, and the difference between the two is used as the combined filter measurements.

3.1. EKF Kalman filter

The extended Kalman filter is a non-linear version of the Kalman filter, which linearizes the process around the operating point, using differentiation. This filter is suitable for applications where the linearization error and degree of non-linearity are low.

$$K(k) = P(k|k-1)H^T[HP(k|k-1)H^T + R]^{-1} \quad (19)$$

$$\hat{x}(k|k) = \hat{x}(k|k-1) + K(k)[y(k) - h(\hat{x}(k|k-1)) \quad (20)$$

$$P(k|k) = [I - K(k)H]P(k|k-1)[I - K(k)H] + K(k)RK^T(k) \quad (21)$$

$$\dot{P}(t|k) = N(\hat{x}(k|k), w_m)P(t|k) + P(t|k)N^T(\hat{x}(k|k), w_m) + M(\hat{x}(k|k), w_m)QM^T(\hat{x}(k|k), w_m) \quad t \in [k\Delta t, (k+1)\Delta t] \quad (22)$$

3.2 UKF Kalman Filter

Using a set of weighted points as sample points, the UKF Kalman filter calculates mea covariance using density distribution. Then these points are mapped by a non-linear transfor function and then their average and covariance are calculated.

The set of sigma points should be selected in such a way that it includes certain information of the probability distribution such as the mean, the error covariance matrix and the slope of the probability distribution, that is, the statistical characteristics of the mean, the error covariance matrix and the slope of the distribution of sigma points are equal to the same characteristics of the random vector x. Of course, it is assumed that the distribution function is Gaussian and among the statistical characteristics of the probability distribution, the goal is to find the mean and the error covariance matrix of the probability distribution. Therefore, the sigma points with the symbol χi and their corresponding weights, Wi, must be prime.

$$\chi_i = \bar{x} + \left(\sqrt{nP_x}\right)_i \quad W_i = \frac{1}{2n} \quad i = 1. \ldots . n \tag{23}$$

$$\chi_{i+n} = \bar{x} - \left(\sqrt{nP_x}\right)_i \quad W_{\mathrm{i+n}} = \frac{1}{2n} \quad i = 1. \ldots . n \tag{24}$$

$$x^a(k|k) = \begin{bmatrix} \hat{x}(k|k) \\ 0 \end{bmatrix} \quad P^a(k|k) = \begin{bmatrix} P(k|k) & P_{xn}(k|k) \\ P_{xn}(k|k) & Q \end{bmatrix} \tag{25}$$

Based on the set of calculations, the estimated state vector and the corresponding covariance matrix are obtained.

$$\widehat{(x}(k+1|k+1) = \hat{x}(k+1|k) + K(k+1)(Y(k+1) - \hat{Y}(k+1|k)) \tag{26}$$

$$P(k+1|k+1) = P(k+1|k) - K(k+1)P_{yy}K^T(k+1) \tag{27}$$

Based on the set of calculations performed, the state vector is estimated and the corresponding covariance matrix is obtained.

$$\hat{x}(k+1|k+1) = \hat{x}(k+1|k) + K(k+1)(Y(k+1) - \hat{Y}(k+1|k)) \tag{28}$$

$$P(k+1|k+1) = P(k+1|k) - K(k+1)P_{yy}K^T(k+1) \tag{29}$$

The algorithm is repeated again from the first step.

Sigma points can be calculated using the Van der Merwe algorithm. The first point is equal to the average value of the input, and the other values are calculated as follows:

$$x_0 = \mu$$

$$x_i = \begin{cases} \mu - \left[\sqrt{n+\lambda\sum}\right]_{i-n} & fori = (n+1)...2n \\ \mu + \left[\sqrt{n+\lambda\sum}\right]_i & fori = 1...n \end{cases} \tag{30}$$

For the updating step, we create a measurement function that converts the sigma points to the measurement space and the updating step is performed in the ineffective Kalman filter:

$$Z = h(y_\sigma) \tag{31}$$

Again, using the ineffective Kalman filter, we give the sigma points and the corresponding weights to the measurement function to calculate the modes and covariance in the measurement space as follows:

$$\begin{aligned} \mu_{z_k} &= \sum_{i-0}^{2n} \omega_i^m z \\ P_{z_k} &= \sum_{i-0}^{2n} \omega_i^c (z-\mu_{z_k})(z-\mu_{z_k})^T + R \end{aligned} \tag{32}$$

3.3 Particle Kalman filter (PKF)

Particle Kalman filter is a combination of Kalman filter and Particle filter in which the solution of the nonlinear problem is checked using the weighted average of a number of parallel Kalman filters. The simultaneous implementation of a number of Kalman filters is heavy from the point of view of computer calculations, and this problem also exists in the Particle filter.

$$p_k^s(x_k|y_{1:k}) = \sum_{i=1}^{N} \omega_k^i N(x_k : x_k^{s,i}, P_k^{s,i}) \tag{33}$$

$$\tilde{p}_{k-1}(x_{k-1}|y_{1:k-1}) = \sum_{i=1}^{N} \tilde{\omega}_{k-1}^i N(x_{k-1} : \theta_{k-1}^i \Phi_{k-1}^i) \tag{34}$$

$$p_k^f(x_k|y_{1:k-1}) = \int_{R^n} N(x_k : M_k(x_{k-1})Q_k) p_{k-1}^a(x_{k-1}|y_{1:k-1}) dx_{k-1} \tag{35}$$

$$\omega_k^i = \frac{\tilde{\omega}_k^i N(y_k : H_k(\hat{x}_k^{f,i})\Sigma_k^i)}{\sum_{j=1}^{N} \tilde{\omega}_{k-1}^i N(y_k : H_k(\hat{x}_k^{f,i})\Sigma_k^i)} \tag{36}$$

Considering this estimator, the Particle Kalman Filter (PKF) will be able to estimate the conditional states in the nonlinear optimal filter using a combination of N Gaussian probability densities in the form of the following equation.

Selecting a set of sigma points

$$\chi_i = \bar{x} + \left(\sqrt{nP_x}\right)_i \quad W_i = \frac{1}{2n} \quad i = 1, \dots, n \tag{37}$$

$$\chi_{i+n} = \bar{x} - \left(\sqrt{nP_x}\right)_i \quad W_{+ni} = \frac{1}{2n} \quad i = 1, \dots, n \tag{38}$$

$$x^a(k|k) = \begin{bmatrix} \hat{x}(k|k) \\ 0 \end{bmatrix} \quad P^a(k|k) = \begin{bmatrix} P(k|k) & P_{xn}(k|k) \\ P_{xn}(k|k) & Q \end{bmatrix} \tag{39}$$

This formula shows that even with noise dependent on the state vector, this filter can be easily used to estimate the state vector.

4. Simulating and Evaluating Performance under GPS Disconnection

The filters were implemented using MATLAB's Function environment for simulation purposes. While some input parameters differ across filters, efforts were made to standardize the input and output of the MATLAB Function block to facilitate seamless replacement of filters. Additionally, global variable definitions were used to make various parameters accessible to the functions. In these simulations, the previous position values (X, Y, Z) and velocities along the three axes were used as state variables for prediction. Feedback from the predicted state was incorporated into the MATLAB Function block to support iterative calculations for subsequent prediction cycles.

The UKF parameters were set to $\alpha = 0.1$, $\beta=2$, $\kappa=0$, with process noise covariance I $Q=0.1I$ and measurement noise $R=0.5I$. For the PKF, 500 particles were used with systematic resampling.

Figures 2 & 3 present the simulation results in four modes during GPS-disrupted conditions. The blue curve represents the system operating in normal mode without any filter, serving as a reference. The black curve shows results with the Extended Kalman Filter (EKF), while the red and green curves correspond to the Unscented Kalman Filter (UKF) and the Particle Kalman Filter (PKF), respectively. The objective of these simulations was to evaluate how closely each filter's results align with the actual feedback from the flying object's position and velocities (blue curve). The filter that produces results most similar to the blue curve is considered to provide the most accurate estimates. To streamline the simulation and facilitate comparisons, the duration was set to 25 seconds. Across all figures, the performance of EKF, UKF, and PKF was analyzed, demonstrating the comparative accuracy of these filters in handling GPS disconnection scenarios.

In table 1, we provide the IMU device parameters used in the simulation experiment, including details on the gyroscope and accelerometer.

Table1. IMU Parameters for Simulation

Gyroscope		Accelerometer	
Angular Random Walk (ARW)	0.01–0.1 °/√hr	Velocity Random Walk (VRW)	50–500 μg/√Hz
Bias Instability	1–10 °/hr	Bias Instability	10–500 μg
Zero Bias (Bias Drift)	0.1–10 °/s	Zero Bias (Bias Drift)	100–1000 μg
Noise Density	0.001–0.02 °/s/√Hz	Noise Density	10–500 μg/√Hz

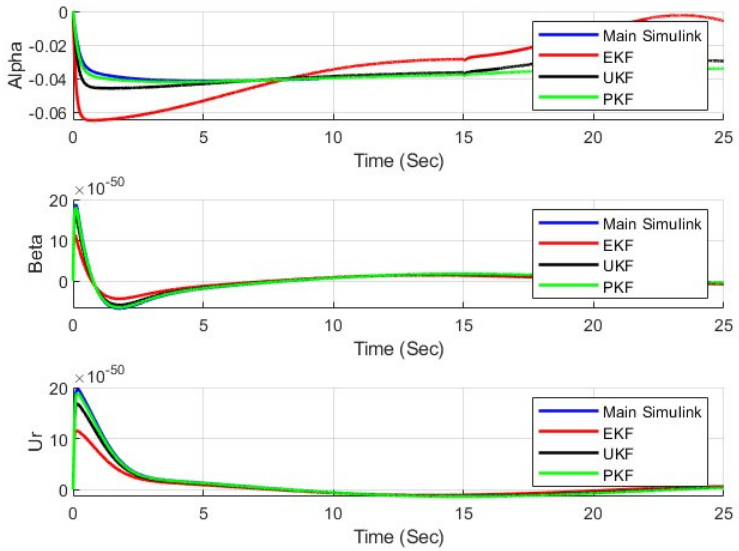

Fig 2. Aerodynamic forces without GPS disconnection

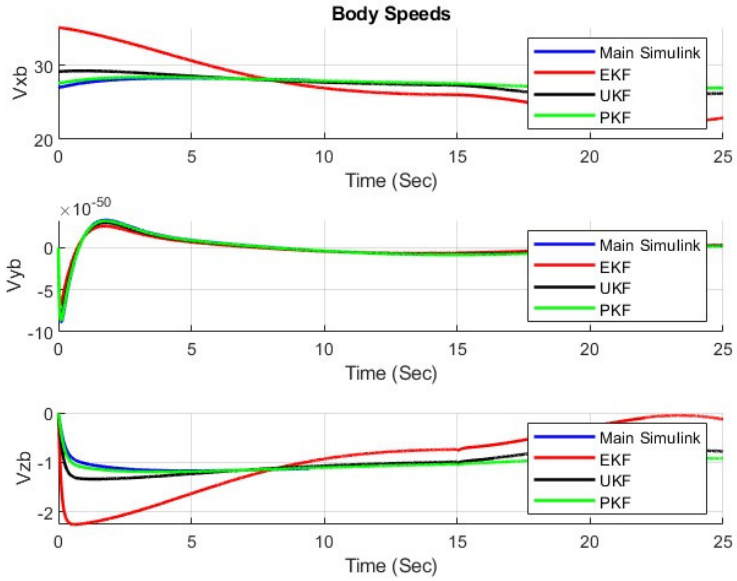

Fig3.body speed without GPS disconnection

Table2. Comparison of control parameters in four simulated modes

Criterion	Parameter	No filter and real feedback	EKF	UKF	PKF
Root Mean Square	Fx deviation from the final value	0.1314	1.0659	0.2513	0.1013

	Fy deviation from the final value	0	0	0	0
	Fz deviation from the final value	0.2982	2.6447	0.6103	0.4401
Root Mean Square	Gx deviation from the final value	0.0862	2.537	0.33	0.1449
	Gy deviation from the final value	0	0	0	0
	Gz deviation from the final value	0.0047	0.6123	0.0315	0.0073
The percentage of mutation	Velocity in the X direction	1.2362	5.0732	56.3589	2.3981
	Velocity in the Y direction	---	---	---	---
	Velocity in the Z direction	11.4462	741.31	25.2314	4.8788

Table 1 presents a numerical comparison of control parameters across four simulated scenarios. The overshoot values of velocity along the Y-axis in all cases are negligible, ranging between 10–50, and are therefore excluded from the table for clarity. From the figures, it is evident that when UKF and PKF filters are applied, the simulation results closely resemble the case where no filter is used, and direct feedback from position and velocities is available. On the contrary, using the EKF filter leads to greater deviation of the parameters from the true values, which is primarily due to the nonlinearity of the system and the suitability of the EKF for linear models. In terms of control inputs, especially Ue and Ur, the deviations are significantly smaller with UKF and PKF compared to EKF or no filter. However, this difference is less pronounced for Ua. Parameters such as engine speed, AOF, and elevator also exhibit smaller errors and deviations when UKF and PKF are used, as opposed to EKF. Table 1 further highlight that the deviation from steady-state values and the percentage of

overshoot in speeds are minimized with UKF and PKF filters compared to cases without filters. This demonstrates their effectiveness in providing accurate feedback to the control system. The EKF, on the other hand, performs less effectively due to its reliance on linearized models, which are unsuitable for systems with significant non-linear dynamics. Overall, UKF and PKF filters prove to be superior for state estimation in non-linear systems, delivering better results with reduced errors and deviations compared to EKF.

4.1. Simulating GPS Disconnection for 15 Seconds

The system simulation results under four scenarios, including a GPS cut-off. The blue curve represents the system operating in normal mode without any filters, serving as the reference. The black, red, and green curves correspond to the results when using the EKF, UKF, and PKF filters, respectively. The simulation aims to evaluate the system's ability to estimate its position and trajectory during a GPS outage when different predictor and estimator filters are employed. The simulation runs for a total duration of 25 seconds, with the GPS being disconnected from the 15th second onwards. This setup allows for a comparative analysis of filter performance during GPS outages, highlighting how effectively each filter maintains accurate position and route estimation under such conditions.

In Figures 4 and 5, where the GPS outage occurs at 15 seconds, the fax plot diverges for the cases where the estimator filter is not used, which is due to the loss of the bird's position feedback, but the plots that use it do. The divergence of Engine Speed and Elevator is quite evident if the estimator is not used. In addition, the error and deviation of the results obtained from EKF is more than UKF and PKF. In the case of AOF, the blue curve (without an estimator) has converged to an incorrect value, which is not observed for other curves (curves with an estimator). In addition, the convergence of UKF and PKF curves has occurred much faster than EKF.

After disconnecting the GPS, the blue position curves (without filter) have reached zero, but the other curves have continued to estimate the route and position. As can be seen, the position estimation for UKF and PKF filters is more appropriate and accurate than EKF and has less error.

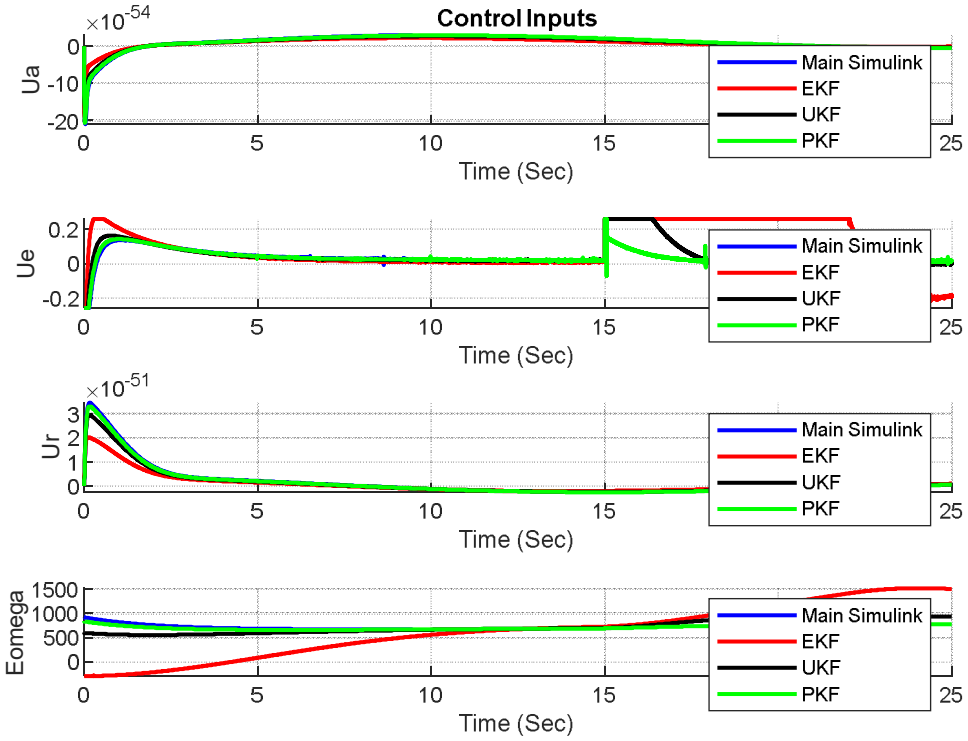

Fig4. Control inputs for GPS cutoff at 15 seconds

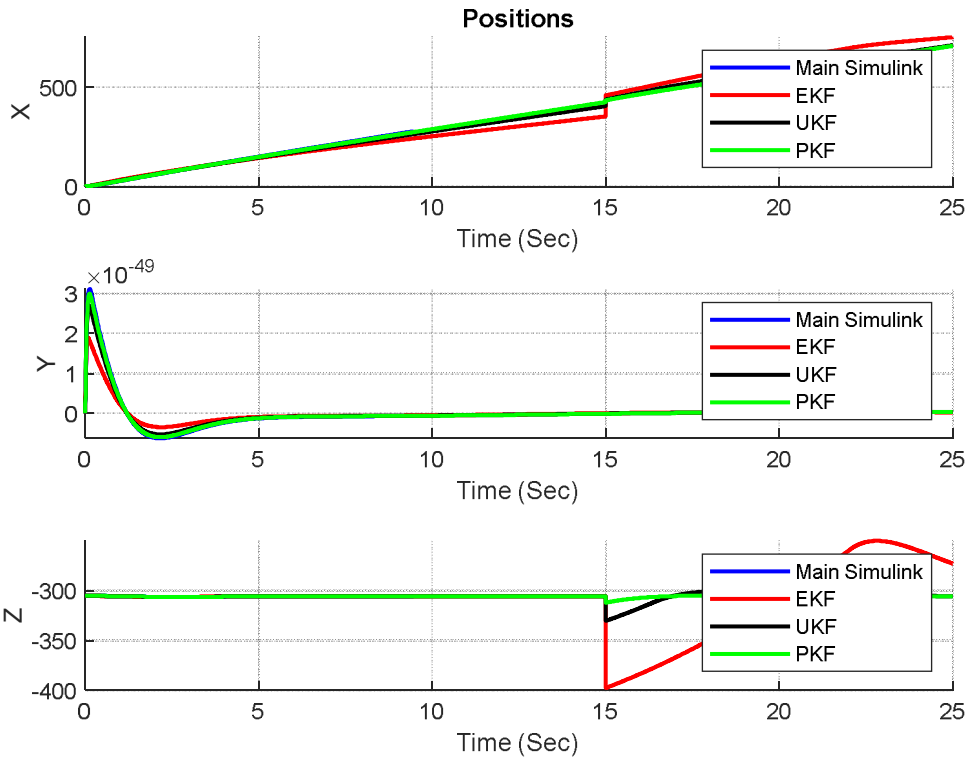

Fig5. Position along X, Y and Z direction of GPS disconnection in 15 seconds

Table 3. Comparison of control parameters in four simulated modes in GPS outage at 15 seconds

Criterion	Parameter	No filter and real feedback	EKF	UKF	PKF
Root Mean Square	Fx deviation from the final value	4.0548	0.4664	0.1145	0.0536
	Fy deviation from the final value	0	0	0	0
	Fz deviation from the final value	1.4949	0.6771	0.2308	0.1798
Root Mean Square	Gx deviation from the final value	1.835	0.8348	0.1443	0.0591
	Gy deviation from the final value	0	0	0	0
	Gz deviation from the final value	0.2589	0.1104	0.0104	0.0049
The percentage of mutation	Velocity in the X direction	Divergence	53.4087	11.6219	5.4411
	Velocity in the Y direction	---	---	---	---
	Velocity in the Z direction	Divergence	1635/3	72/0926	29/7413

Table 2 also shows that the deviation of the parameters from the value of the steady state and the percentage of overshoot of the velocities is very small in the case of using UKF and PKF filters and in the condition of GPS disconnection. If no estimation filter is used and GPS is disconnected, the parameters under investigation will diverge. Also, the use of the extended

Kalman filter (EKF) does not seem appropriate due to the need for a linearized model and the existence of many nonlinear factors in the system. In general, UKF and PKF filters, considering that they are more suitable for state estimation in nonlinear systems, lead to better results and have less error and less deviation compared to EKF. In the comparison between PKF and UKF, PKF has usually provided a more appropriate response and behavior. Also, as seen in Figure 7, by using PKF and UKF filters, the path and position of the bird object have been tracked correctly and with a small error (much less than 500 meters)

4.2. Simulating GPS Disconnection for 5 Minutes

To evaluate the system's behavior during extended GPS disconnection, simulations were conducted for 315 seconds, with the GPS being disconnected from the 15th second until the end of the simulation (equivalent to 5 minutes). Given the results from previous sections, it was observed that without a prediction filter or when using the EKF, prolonged GPS outages cause system divergence. Therefore, only the UKF and PKF, which demonstrated more favorable responses, were considered for this extended simulation. Running the simulation with UKF and PKF under these conditions requires approximately 1 hour and 30 minutes. To improve efficiency, the Charts block was removed, with all simulation data stored in the designated folder for later analysis. The results are presented in Figures 6-7, highlighting the performance differences between the UKF and PKF filters during the extended GPS disconnection period. These simulations further reinforce the advantages of UKF and PKF in handling nonlinear systems, ensuring system stability and accurate state estimation over prolonged GPS outages.

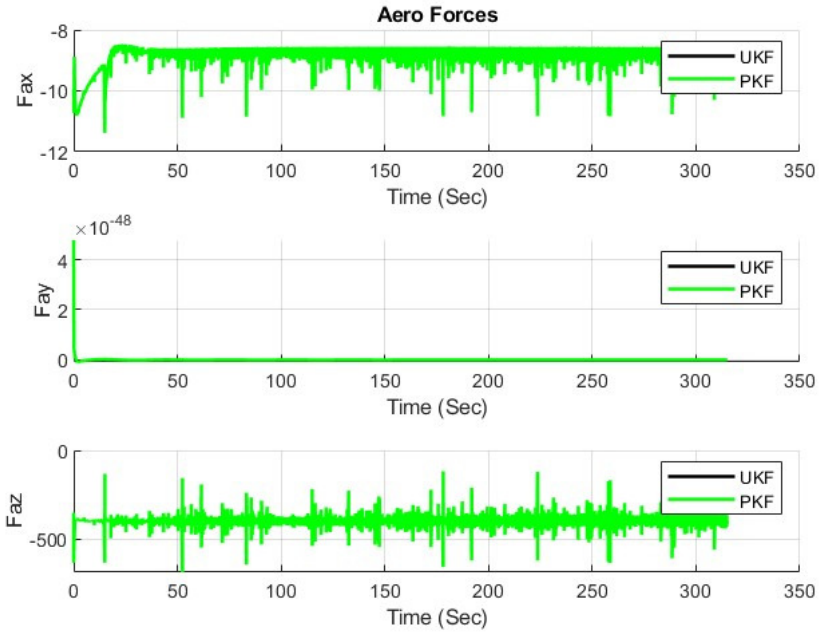

Fig6. Aerodynamic forces in the X, Y and Z direction of GPS disconnection for 5 minutes

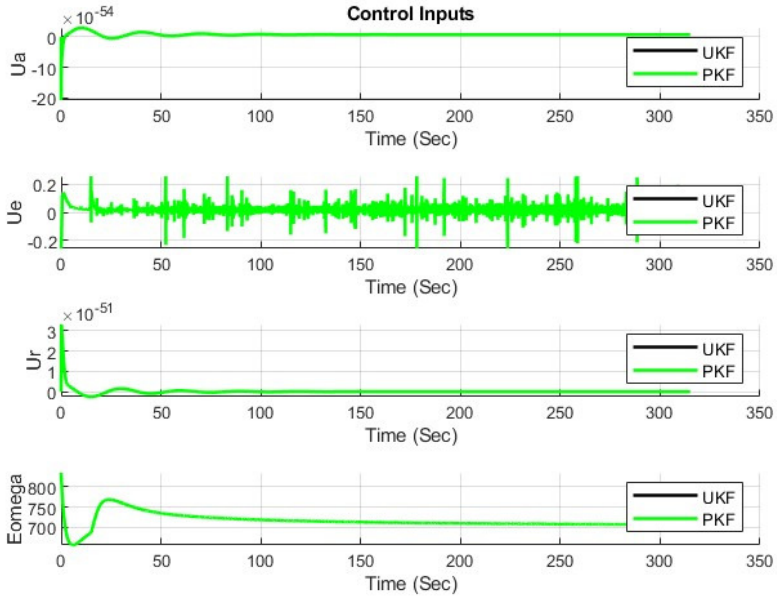

Fig7. Control inputs to cut off GPS for 5 minutes

In the analysis of the results of the 315-second vote simulation, where the GPS was cut off from the 15th to the last second, it can be said that according to Figure 6, the PKF filter compared to the UKF led to faster convergence and less error compared to the value It has become final.

Table 4. Comparison of control parameters in four simulated situations of GPS disconnection for 5 minutes

Criterion	Parameter	UKF	PKF
Root Mean Square	Fx deviation from the final value	0/0018	0/0011
	Fy deviation from the final value	0	0
	Fz deviation from the final value	0/043	0/0235
Root Mean Square	Gx deviation from the final value	0/0051	0/0018
	Gy deviation from the final value	0	0
	Gz deviation from the final value	0/0056	0/0057
The percentage of mutation	Velocity in the X direction	8/337	5/1873

	Velocity in the Y direction	---	---
	Velocity in the Z direction	38/7196	23/8822

Table 3 also shows that the deviation of the parameters from the value of the steady state and the percentage of overshoot of the velocities when using the PKF filter is somewhat lower than the UKF. Therefore, it can be said that when comparing PKF and UKF, PKF has provided a more appropriate response and behavior. Also, as seen in Figure 6, by using PKF and UKF filters, the path and position of the bird object have been tracked correctly and with a small error (much less than 500 meters).

5. Conclusion

This study investigated the limitations of inertial navigation systems (INS) in accurate position estimation, particularly during GPS outages or high-error scenarios. By integrating INS with GPS data and employing advanced nonlinear Kalman filters including the Particle Kalman Filter (PKF) and Unscented Kalman Filter (UKF) we achieved significant improvements in accuracy and reliability. The PKF, leveraging particle filter properties, exhibited the fastest convergence and superior tracking performance compared to the UKF and EKF. Our results demonstrated that Kalman filtering effectively prevents autopilot divergence during GPS disconnections, reducing positional error to negligible levels. While the PKF's computational demands remain a consideration, its robustness underscores its potential for real-world applications. Future research could explore hybrid approaches, combining nonlinear filters with machine learning to enhance real-time adaptability in GPS-denied environments. Such advancements would be pivotal for autonomous systems, from drones to self-driving vehicles, ensuring precision even under challenging conditions.

Data Availability. Data underlying the results presented in this paper are available from the corresponding author upon reasonable request.

Funding. There is no funding for this work.

Conflicts of interest. The authors declare no conflict of interest.

Ethics. The authors declare that the present research work has fulfilled all relevant ethical guidelines required by COPE.

References:

[1] L. Marković, M. Kovač, R. Milijas, M. Car, and S. Bogdan. “Error state extended kalman filter multi-sensor fusion for unmanned aerial vehicle localization in gps and magnetometer denied indoor environments.”. International Conference on Unmanned Aircraft Systems (ICUAS) IEEE, pp. 184–190, 2022. DOI: https://doi.org/10.1109/ICUAS54217.2022.9836124.

[2] W. Wan, H. Kim, N. Hovakimyan, P. Voulgaris, and L. R. Sha. “Resilient Estimation and Safe Planning for UAVs in GPS-Denied Environments. In Control of Autonomous Aerial Vehicles.”. Advances in Autopilot Design for Civilian UAVs, Cham: Springer Nature Switzerland, pp. 167–193, 2023. DOI: https://doi.org/10.1007/978-3-031-39767-7_7

[3] S. B. Kim, J. C. Bazin, H. K. Lee, K. H. Choi, and S. Y. Park. “Ground vehicle navigation in harsh urban conditions by integrating inertial navigation system, global positioning system, odometer and vision data.”. IET radar, sonar & navigation, 5(8):pp. 814–823, 2011. DOI: https://doi.org/10.1049/iet-rsn.2011.010.

[4] Y. Xiong, Y. Zhang, X. Guo, C. Wang, C. Shen, J. Li, J. Tang, and J. Liu. “Seamless global positioning system/inertial navigation system navigation method based on square-Root cubature Kalman filter and random forest regression.”. Review of Scientific Instruments, 90(1), 2019. DOI: https://doi.org/10.1063/1.5079889.

[5] Cao, H., Li, H., Shao, X., Liu, Z., Kou, Z., Shan, Y., Shi, Y., Shen, C. and Liu, J.,. “Sensing mode coupling analysis for dual-mass MEMS gyroscope and bandwidth expansion within wide-temperature range. Mechanical Systems and Signal Processing,” 98, pp.448-464. 2018. DOI: https://doi.org/10.1016/j.ymssp.2017.05.003

[6] Liu, X., Zhao, Y., Liu, X., Yang, Y., Song, Q. and Liu, Z.,. “An improved self-alignment method for strapdown inertial navigation system based on gravitational apparent motion and dual-vector. Review of Scientific Instruments”, 85(12), p.125108. 2014. DOI: https://doi.org/10.1063/1.4903196

[7] Guo, X., Sun, C., Wang, P. and Huang, L.,. “Vision sensor and dual MEMS gyroscope integrated system for attitude determination on moving base”. Review of Scientific Instruments, 89(1), p.015002. 2018 DOI: https://doi.org/10.1063/1.5011703

[8] Bhatt, D., Aggarwal, P., Devabhaktuni, V. and Bhattacharya, P.,. “A novel hybrid fusion algorithm to bridge the period of GPS outages using low-cost INS. Expert Systems with Applications”, 41(5), pp.2166-2173. 2014 DOI: https://doi.org/10.1016/j.eswa.2013.09.015

[9] Enkhtur, M., Cho, S.Y. and Kim, K.H.,. “Modified unscented Kalman filter for a multirate INS/GPS integrated navigation system”. Etri Journal, 35(5), pp.943-946. 2013. DOI: https://doi.org/10.4218/etrij.13.0212.0540

[10] Xu, Q., Li, X. and Chan, C.Y.,.”A cost-effective vehicle localization solution using an interacting multiple model– unscented Kalman filters (IMM-UKF) algorithm and grey neural network. Sensors”, 17(6), p.1431. 2017 DOI: https://doi.org/10.3390/s17061431

[11] Cui, B., Chen, X. and Tang, X.,. “Improved cubature Kalman filter for GNSS/INS based on transformation of posterior sigma-points error. IEEE Transactions on Signal Processing”, 65(11), pp.2975-2987. 2017. DOI: https://doi.org/10.1109/TSP.2017.2679685

[12] Havyarimana, V., Hanyurwimfura, D., Nsengiyumva, P. and Xiao, Z.,. “A novel hybrid approach based-SRG model for vehicle position prediction in multi-GPS outage conditions”. Information Fusion, 41, pp.1-8. 2018. DOI: https://doi.org/10.1016/j.inffus.2017.07.002

[13] Jiang, C., Zhang, S.B. and Zhang, Q.Z.,. “Adaptive estimation of multiple fading factors for GPS/INS integrated navigation systems. Sensors”, 17(6), p.1254. 2017. DOI: https://doi.org/10.3390/s17061254

[14] Zhang, Y., Shen, C., Tang, J. and Liu, J.,. “Hybrid algorithm based on MDF-CKF and RF for GPS/INS system during GPS outages” (April 2018). IEEE Access, 6, pp.35343-35354. 2018. DOI: https://doi.org/10.1109/ACCESS.2018.2849217

[15] Yao, Y., Xu, X., Zhu, C. and Chan, C.Y.,. “A hybrid fusion algorithm for GPS/INS integration during GPS outages. Measurement”, 103, pp.42-51. 2017. DOI: https://doi.org/10.1016/j.measurement.2017.01.053

[16] Li, J., Song, N., Yang, G., Li, M. and Cai, Q.“Improving positioning accuracy of vehicular navigation system during GPS outages utilizing ensemble learning algorithm. Information Fusion”, 35, pp.1-10. 2017, DOI: https://doi.org/10.1016/j.inffus.2016.08.001

[17] Shen, C., Zhang, Y., Guo, X., Chen, X., Cao, H., Tang, J., Li, J. and Liu, J.,. “Seamless GPS/inertial navigation system based on self-learning square root cubature Kalman filter”. IEEE Transactions on Industrial Electronics, 68(1), pp.499-508. 2020. DOI: https://doi.org/10.1109/TIE.2020.2967671

[18] Xu, Y., Shmaliy, Y.S., Chen, X., Li, Y. and Ma, W.,. “Robust inertial navigation system/ultra-wide band integrated indoor quadrotor localization employing adaptive interacting multiple model-unbiased finite impulse response/Kalman filter estimator. Aerospace Science and Technology”, 98, p.105683. 2020, DOI: https://doi.org/10.1016/j.ast.2020.105683

[19] Chen, K., Zhou, J., Shen, F.Q., Sun, H.Y. and Fan, H.,. “Hypersonic boost–glide vehicle strap down inertial navigation system/global positioning system algorithm in a launch-centered earth-fixed frame. Aerospace science and technology”, 98, p.105679. 2020. DOI: https://doi.org/10.1016/j.ast.2020.105679

[20] Lu, H., Shen, H., Tian, B., Zhang, X., Yang, Z. and Zong, Q.,. “Flight in GPS-denied environment: Autonomous navigation system for micro-aerial vehicle. Aerospace Science and Technology”, 124, p.107521. 2022. DOI: https://doi.org/10.1016/j.ast.2022.107521

[21] Liu, N., Su, Z., Li, Q., Zhao, H. and Qi, W.,. “A combined ckf-psr method for random noise compensation of vibratory gyroscopes. Journal of Industrial Information Integration”, 25, p.100241. 2022. DOI: https://doi.org/10.1016/j.jii.2021.100241

[22] Zhang, S., Tu, R., Gao, Z., Zhang, P., Wang, S. and Lu, X.,. “Low-Earth-Orbit Satellites and Robust Theory-Augmented GPS/Inertial-Navigation-System Tight Integration for Vehicle-Borne Positioning. Electronics”, 13(3) p.508., 2024. DOI: https://doi.org/10.3390/electronics13030508

[23] El-Sheimy, N. and Youssef, A.,. “Inertial sensors technologies for navigation applications: State of the art and future trends. Satellite Navigation”, 1(1), p.2. 2020. DOI: https://doi.org/10.1186/s43020-019-0001-5

[24] Cui, B., Wei, X., Chen, X., Wang, A. “Distributionally Robust Kalman Filtering for INS/GPS Tightly Coupled Integration With Model Uncertainty and Measurement Outlier” 2024' DOI: https://doi.org/10.1109/TIM.2023.3293566

[25] Zhao, Y., Liu, J., Tang, W., Zhang, C. (2024) “Novel Augmented Quaternion UKF for Enhanced Loosely Coupled GPS/INS”. DOI: https://doi.org/10.1109/TCST.2024.3425211

[26] Cheng J, Chen H, Xue Z, Huang Y, Zhang Y "An online exploratory maximum likelihood estimation approach to adaptive Kalman filtering". IEEE/CAA Journal of Automatica Sinica. 2024 Dec 24. DOI: 10.1109/JAS.2024.125001

[27] Zhu F, Zhang S, Li X, Huang Y, Zhang Y."Adaptive Kalman Filters With Small-Magnitude and Inaccurate Process Noise Covariance Matrix" Part II: Application to Inertial-Based Integrated Navigation. IEEE Transactions on Aerospace and Electronic Systems. 2025 Jan 28. DOI: 10.1109/TAES.2025.3535481

[28] Zhu F, Huang Y, Xue C, Mihaylova L, Chambers J "A sliding window variational outlier-robust Kalman filter based on student’s t-noise modeling". IEEE Transactions on Aerospace and Electronic Systems. 2022 Apr 1;58(5):4835-49. DOI: 10.1109/TAES.2022.3164012

[29] Du S, Huang Y, Wen W, Zhang Y. "A novel consistent-robust SINS/GNSS/NHC integrated navigation method for autonomous vehicles under intermittent GNSS outage". IEEE Transactions on Intelligent Vehicles. 2024 May 29. DOI: 10.1109/TIV.2024.3406756

[30] Du S, Huang Y, Wen W, Zhang Y. "A Novel Lie Group-based Reliable IMM Estimation Method for SINS/GNSS/OD/NHC Integrated Navigation in Complex Environments". IEEE Internet of Things Journal. 2025 Jan 9. DOI: 10.1109/JIOT.2025.3527555

[31] Cui, B., Wei, X., Chen, X. and Wang, A.”Improved high-degree cubature Kalman filter based on resampling-free sigma-point update framework and its application for inertial navigation system-based integrated navigation. Aerospace Science and Technology”, 117, p.106905. 2021. DOI: https://doi.org/10.1016/j.ast.2021.106905

APPENDIX

Fx, Fy and Fz	aerodynamic forces
T	propulsive force
Ix, Iy and Iz and Ixz	moments of inertial
φ, θ and ψ	attitude angles
α	angle of attack
β	angle of the lateral head
δa	control surface of aileron
δe	control surface of elevator
δr	Rudder control surface
ρ	air density
CL	lift coefficient
CD	drag coefficient
S	wing reference surface
Q	dynamic pressure
Cx, Cy and Cz	aerodynamic force coefficients
$\bar{c}$	average chord
b	length Wing span
Cl, Cm and Cn	coefficients of aerodynamic moment
L	push force
D	pull force
ψ	rotation around the z-axis of the body is the side
θ	y-axis of the body is the twist angle
φ	rotation around the x-axis of the body is the roll angle